MOLECULAR IMAGING AND BIOLOGY

Mol Imaging Biol (2017) 19:24–30
DOI: 10.1007/s11307-016-0985-2

Published Online: 1 August 2016

RESEARCH ARTICLE

MR-Guided Delivery of Hydrophilic Molecular Imaging Agents Across the Blood-Brain Barrier Through Focused Ultrasound

Raag D. Airan,[1] Catherine A. Foss,[1] Nicholas P. K. Ellens,[1] Yuchuan Wang,[1] Ronnie C. Mease,[1] Keyvan Farahani,[1,2] Martin G. Pomper[1]

[1]*The Russell H. Morgan Department of Radiology and Radiological Science, Johns Hopkins Medical Institutions, Baltimore, MD, USA*
[2]*National Cancer Institute, National Institutes of Health, Bethesda, MD, USA*

Abstract

Purpose: A wide variety of hydrophilic imaging and therapeutic agents are unable to gain access to the central nervous system (CNS) due to the blood-brain barrier (BBB). In particular, unless a particular transporter exists that may transport the agent across the BBB, most agents that are larger than 500 Da or that are hydrophilic will be excluded by the BBB. Glutamate carboxypeptidase II (GCPII), also known as the prostate-specific membrane antigen (PSMA) in the periphery, has been implicated in various neuropsychiatric conditions. As all agents that target GCPII are hydrophilic and thereby excluded from the CNS, we used GCPII as a platform for demonstrating our MR-guided focused ultrasound (MRgFUS) technique for delivery of GCPII/PSMA-specific imaging agents to the brain.

Procedures: Female rats underwent MRgFUS-mediated opening of the BBB. After opening of the BBB, either a radio- or fluorescently labeled ureido-based ligand for GCPII/PSMA was administered intravenously. Brain uptake was assessed for 2-(3-{1-carboxy-5-[(6-[^{18}F]fluoro-pyridine-3-carbonyl)-amino]-pentyl}-ureido)-pentanedioic acid ([^{18}F]DCFPyL) and YC-27, two compounds known to bind GCPII/PSMA with high affinity, using positron emission tomography (PET) and near-infrared fluorescence (NIRF) imaging, respectively. Specificity of ligand binding to GCPII/PSMA in the brain was determined with co-administration of a molar excess of ZJ-43, a compound of the same chemical class but different structure from either [^{18}F]DCFPyL or YC-27, which competes for GCPII/PSMA binding.

Results: Dynamic PET imaging using [^{18}F]DCFPyL demonstrated that target uptake reached a plateau by ~1 h after radiotracer administration, with target/background ratios continuing to increase throughout the course of imaging, from a ratio of ~4:1 at 45 min to ~7:1 by 80 min. NIRF imaging likewise demonstrated delivery of YC-27 to the brain, with clear visualization of tracer in the brain at 24 h. Tissue uptake of both ligands was greatly diminished by ZJ-43 co-administration, establishing specificity of binding of each to GCPII/PSMA. On gross and histological examination, animals showed no evidence for hemorrhage or other deleterious consequences of MRgFUS.

Conclusions: MRgFUS provided safe opening of the BBB to enable specific delivery of two hydrophilic agents to target tissues within the brain. This platform might facilitate imaging and therapy using a variety of agents that have heretofore been excluded from the CNS.

Key words: MRgFUS, Blood-brain barrier, GCPII, PSMA, NIRF

Correspondence to: Martin Pomper; *e-mail:* mpomper@jhmi.edu

Introduction

The blood-brain barrier (BBB) excludes many molecular imaging and theranostic agents from the central nervous system (CNS) [1]. For example, the BBB substantially excludes from the CNS probes for the target glutamate carboxypeptidase II (GCPII), which has been implicated in a wide range of neurological and psychiatric disorders such as gliomas [2]; Alzheimer's dementia [3]; and the neurotoxicity associated with schizophrenia, trauma, stroke, and pain [4]. We and others have developed a variety of radioactive and fluorescent compounds that allow imaging of GCPII, known as the prostate-specific membrane antigen (PSMA) in the periphery, in preclinical studies and in men with prostate cancer [5–9]. However, *in vivo* biodistribution studies in both rodents [10] and in humans [5] have demonstrated that these agents are excluded from the brain despite the presence of a significant concentration of GCPII/PSMA on astrocytes [11–13]. Use of isosteres in place of hydrophilic moieties and prodrugs has not adequately increased the concentration of GCPII inhibitors that enter the CNS [14, 15]. We describe a method for molecular imaging of GCPII/PSMA inside the CNS by relaxing the BBB.

Here, we leverage advances in magnetic resonance-guided focused ultrasound (MRgFUS) to overcome the exclusion by the BBB of hydrophilic—in some cases charged—and large (> 500 Da) compounds. Protocols for safe, effective, and reversible opening of the BBB have recently been described for a range of animal models including rodents [16, 17], rabbits [18], and non-human primates [19]. One group has recently performed the first clinical protocol using BBB opening [20]. This technology has proved promising for delivering small molecules [21], antibodies [22], viruses [23], nanoparticles [16], and even cells [24] to the CNS. However, MRgFUS BBB opening for molecular imaging and theranostics has been relatively unexplored. Specifically, we show that we can deliver hydrophilic compounds targeting GCPII/PSMA to the brain using MRgFUS BBB opening. We further show that such targeting is specific. We anticipate that MRgFUS BBB opening will be useful in other, similar situations where there is a need for hydrophilic and/or large species to traverse the BBB for imaging and therapy.

Materials and Methods

Animals and Focused Ultrasound

All procedures using live animals were conducted under a Johns Hopkins University ACUC-approved animal protocol. Female Fischer 344 rats (Charles River Laboratories, Wilmington, MA) between 150 and 250 g were utilized. The rats were housed in a specific pathogen-free facility under a 12/12 light/dark cycle and had free access to water and food ad libitum. Animals were anesthetized with isoflurane (up to 4–5 % for induction and 2 % maintenance, each in medical air at 2 l/min, as supplemental oxygen has been shown to reduce the circulation time of the microbubbles that are critical to the BBB opening procedure [25]), and a 24-G tail vein catheter was placed. The dorsal scalp fur was removed with a chemical depilatory (Veet, RB Group, amazon.com). The animal was placed supine on the bed of a focused ultrasound transducer (RK300, FUS Instruments, Toronto, Canada) that was integrated with a 9.4-T horizontal bore MRI (Bruker BioSpin, Billerica, MA). Ultrasound coupling gel and a vendor-provided water pad were used to couple the dorsal surface of the head to the ultrasound transducer. Following placement, initial planning and target selection were completed with T1- and T2-weighted MRI images, with assurance *via* MRI of no significant air bubbles in the path of the ultrasound. If bubbles were visible in the beam path, the animal was repositioned to exclude these bubbles. Following this planning MRI, the animals were administered microbubbles (6×10^3 bubbles/g; Definity, Lantheus Medical Imaging, N. Billerica, MA) *via* the tail vein catheter, and simultaneously (as microbubbles have a short, 2–3-min biological half-life [25]), sonication (1 MHz; 10 ms pulses/1 s × 120 s; 0.45–0.55-MPa estimated *in situ* pressure) was applied to intracranial foci selected from the planning images. Notably, the *in situ* pressure was estimated *via* the method of [26] to account for the attenuation due to rat skull, although the attenuation due to microbubble-perfused skin is unknown in this context and may be significant [27]. Overall, this method is an adaptation of those published previously [28] and uses sonication intensities and pressures similar to those of other more recent studies [16]. Following sonication, gadolinium-based contrast (0.2 μl/g; Magnevist, Bayer, Whippany, NJ) was administered intravenously with BBB opening confirmed with high signal on subsequent post-contrast T1-weighted MRI.

PET/CT Imaging and Ex Vivo Analysis

A total of five rats underwent dynamic positron emission tomography (PET) imaging following BBB opening. Each animal was maintained under anesthesia with 2.5 % isoflurane in oxygen (2 l/min) and positioned in a small animal SuperArgus PET/CT system (Sedecal, Madrid, Spain). After 20 min from BBB opening, to allow clearance of gadolinium and the microbubbles from the blood pool [29, 30], each rat was administered 9.1 MBq (246 μCi) of 2-(3-{1-carboxy-5-[(6-[^{18}F]fluoro-pyridine-3-carbonyl)-amino]-pentyl}-ureido)-pentanedioic acid ([^{18}F]DCFPyL) [5] intravenously as a bolus, with one rat receiving a co-administration of 8 mg/kg of (*S*)-2-(3-((*S*)-1-carboxy-3-methylbutyl)ureido)pentanedioic acid (ZJ-43) (Tocris Bioscience, Bristol, UK) [14]. Dynamic PET imaging started simultaneously with dose administration and proceeded for 2 h, with the imaging field of view centered over the brain. A CT scan utilizing 360 projections at 60 keV was performed for anatomic co-registration purposes. Dynamic PET data were reconstructed using the manufacturer-provided 2D OSEM algorithm [31], and CT data were reconstructed with a manufacturer-provided standard filtered back-projection method. The PET reconstructed images were first co-registered with the CT and subsequently with the post-contrast T1-weighted MRI acquired following MRgFUS BBB opening, through manual alignments based on anatomical landmarks using the software package PMOD (PMOD Technologies LTD, Zürich, Switzerland). The target foci were readily identified on both

MRI and PET. The target with the highest PET uptake in each rat (at 60 min post-injection) was quantified by using a spherical region of interest (2 mm in radius) centered on each focus and compared to that in a background region of the brain. The time-activity curves, depicting the average regional radiotracer concentration at different time points after injection, were obtained for both the target and background regions. Subsequently, the time-wise target to background ratios were calculated.

Ex Vivo Autoradiography

Twenty minutes following BBB opening, one rat was injected intravenously with 30.71 MBq (830 μCi) of [^{18}F]DCFPyL and allowed to undergo a 2-h conscious uptake period prior to isoflurane-enabled euthanasia by cervical dislocation. The brain was then rapidly removed, and selected regions were serially sectioned on a cryotome (HM Microm 550, Thermo Scientific, Waltham, MA) to 20-μm thickness in the coronal plane and annealed to charged glass slides (VWR Scientific, Philadelphia, PA). The slides were dried in air and then exposed to X-ray film (Kodak Biomax, Fisher Scientific, Waltham, MA) for 24 h. The film was then digitized using an MCID densitometry system (Nottingham, UK) and grossly aligned to the Franklin and Paxinos 3rd Ed. The Mouse Brain Atlas (Academic Press, ISBN 978-0-12-374261-2). The corresponding 6th Ed. Rat brain axis is in axial format only.

Near IR Optical Imaging and Ex Vivo Analysis

Following BBB opening, four additional rats were intravenously administered the fluorescent GCPII probe 2-((*E*)-2-((*E*)-3-((*E*)-2-(3,3-dimethyl-5-sulfo-1-(4-sulfobutyl)indolin-2-ylidene)ethylidene)-2-(4-sulfophenoxy)cyclohex-1-enyl)vinyl)-3,3-dimethyl-1-((3*S*,7*S*)-1,3,7,22-tetracarboxy-5,13,20,28-tetraoxo-4,6,12,21,27-pentaazatritriacontan-33-yl)-3H-indolium-5-sulfonate (YC-27; 1 nmol; LI-COR Biosciences, Lincoln, NE) [32] with or without the pharmacological blocker ZJ-43 (5 mg/kg IV) [14]. After 24 h, the rats were euthanized by cervical dislocation under isoflurane anesthesia and their dorsal calvaria were removed to reveal the brain. The heads were imaged using a LI-COR Biosciences optical imaging system using white light and 800-nm emission filter. Images were obtained using the manufacturer's software. Immediately following imaging, the brains were then harvested and frozen on dry ice prior to sectioning on a cryotome (HM Microm 550) to 20-μm thickness and mounting on glass slides (VWR). The slides were then subjected to whole-mount imaging using a LI-COR Odyssey imager capturing both 800-nm emissions (YC-27) and 710-nm emissions for tissue (porphyrin autofluorescence) background.

Results

MRgFUS Site Specifically Opens the BBB

Using the described methods (Fig. 1), we can reliably induce BBB opening with an MR-guided focused ultrasound (MRgFUS) setup. Focal spots of high signal on the post-contrast T1-weighted (T1w) MRI images demonstrated foci of gadolinium-based contrast extravasation past the BBB. Notably, in agreement to what has been shown previously [16, 19, 33, 34], on either MRI completed after the BBB opening procedure or any of the histological studies described below, there was no visible evidence of hematoma formation or other significant deleterious consequences of this procedure.

Dynamic PET-CT Imaging of [^{18}F]DCFPyL Delivery to Healthy Brain

Following MRgFUS BBB opening, the rats were administered an intravenous bolus of [^{18}F]DCFPyL, and PET/CT data were acquired 2 h after radiotracer injection. For rats that displayed successful BBB opening (as assessed with high T1w signal at the targets on post-contrast MRI) and were administered [^{18}F]DCFPyL alone, radiotracer activity was found to localize exactly to the foci of BBB opening (Fig. 2a). Those foci of radiotracer activity were oriented along the dorsal-ventral columns that are expected for the sonication pressure fields of the MRgFUS transducer in use for this study. Radioactivity extended minimally beyond the foci of gadolinium-based contrast accumulation indicating penetration to the brain interstitial space. Beyond the foci of BBB opening, radiotracer was found only in regions of blood pool or where a BBB is not complete, like

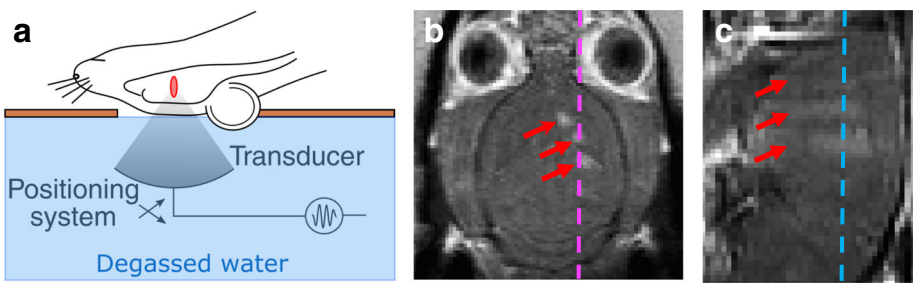

Fig. 1 MR-guided focused ultrasound (MRgFUS)-mediated opening of the BBB. **a** Schematic showing the relative position of the rat head and brain with respect to the transducer face and the resultant sonication focus (*red ellipse*) in the brain. Typical results after BBB opening assessed by post-contrast T1w MRI (presented in the native resolution of the MRI) in the **b** coronal and **c** sagittal planes demonstrate contrast crossing the BBB in three sonication foci (*red arrows*) in the left hemisphere. *Dashed lines* indicate the plane of the right, sagittal (*magenta*) and the middle, coronal (*cyan*) images (Color figure online).

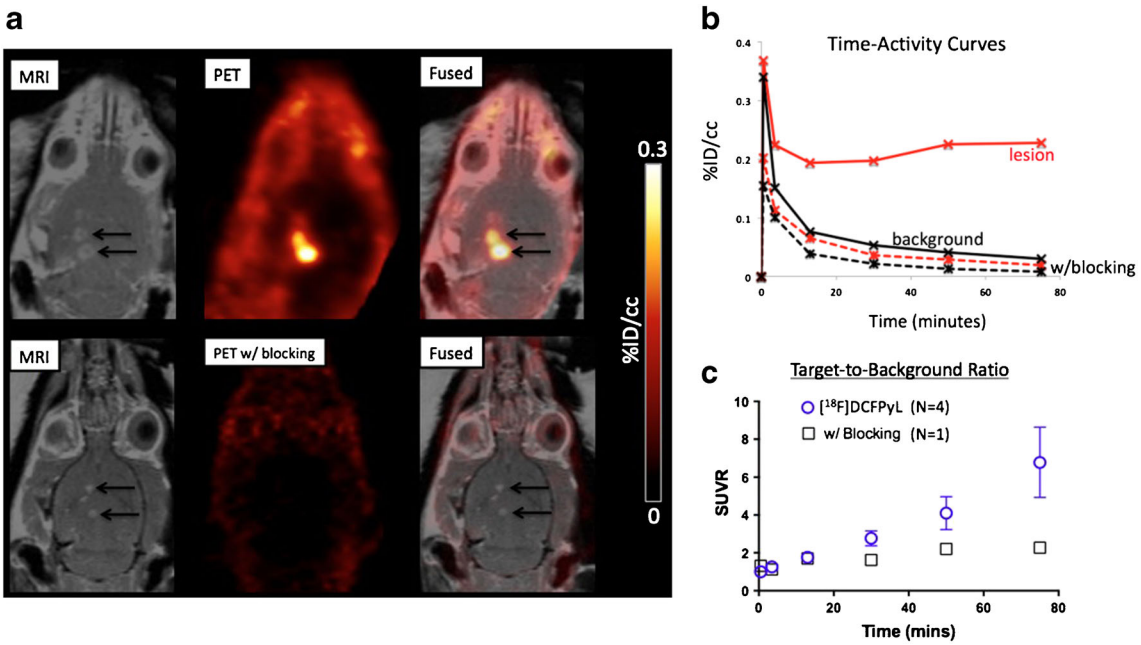

Fig. 2 Delivery of [^{18}F]DCFPyL to the CNS. **a** Coronal T1-weighted post-contrast MRI (*left*), PET (*middle*), and PET-MRI overlay (*right*) demonstrate delivery of [^{18}F]DCFPyL alone (*top row*) or with ZJ-43 (*bottom row*), a competitor for GCPII binding, to the targets of BBB opening. **b** Time-activity curves for PET-CT imaging of [^{18}F]DCFPyL alone (*solid curves*) or with the blocking agent ZJ-43 (*dashed curves*) delivered to BBB opening targets (*red curves*) *vs*. background regions of interest (*black curves*). **c** SUV ratios (SUVR) of target to background *vs*. time for PET-CT imaging following MRgFUS BBB opening and administration of [^{18}F]DCFPyL alone (*blue circles*; presented as mean ± standard deviation) or with the blocking agent ZJ-43 (*black squares*) (Color figure online).

the pituitary gland and cavernous sinus. Time-activity curves (Fig. 2b) established that the target uptake without blocking reached a plateau approximately 1 h post-radiotracer administration, with background activity continuing to diminish over the course of imaging, resulting in a generally increasing target to background ratio (Fig. 2c) over 2 h, with a target to background ratio of approximately 7:1 by 80 min.

ZJ-43 effectively blocked [^{18}F]DCFPyL uptake in peripheral sites of GCPII-expressing tissues [10] and contains the same BBB-excluded tri-carboxylic acid pharmacophore [35]. The target to background ratio in the ZJ-43 co-administration blocking study was four times lower by the end of dynamic PET imaging, indicating that [^{18}F]DCFPyL brain localization was specific to GCPII (Fig. 2c). Autoradiography following MRgFUS BBB opening with varying estimated *in situ* pressures and intravenous administration of [^{18}F]DCFPyL (Fig. 3) also confirmed the delivery into the brain parenchyma of the tracer, with penetration beyond the expected extent of the threshold sonication field.

Near IR Fluorescence Imaging of YC-27 Uptake

We performed similar imaging studies on rats with BBB opening using the GCPII-specific near IR fluorescent compound YC-27 [32], with or without co-administration of ZJ-43. Near IR fluorescence (NIRF) imaging provides high-resolution, quantitative localization of tracer deposition for each brain structure. Fluorescent tracers also allow for longer uptake times and duration of probe retention without the signal limitation seen with radionuclide decay. After opening of the BBB rats were injected with 1 nmol of YC-27 ± ZJ-43 and sacrificed 24 h after injection. After removing the calvarium to reduce scatter and attenuation, each head was photographed and showed intense, highly focused uptake of YC-27 in the brain that co-localized precisely with the gadolinium extravasation into the CNS that was seen following BBB opening (Fig. 4). Whole-mount sections of the brains were scanned again to obtain high-resolution uptake patterns and for quantitation of ipsilateral to contralateral tracer uptake. Rats that were co-injected with ZJ-43 showed a 64 % reduction of YC-27 uptake that also tightly co-localized with T1w gadolinium infiltration. YC-27 uptake in regions where the BBB was opened was tenfold higher than in the corresponding contralateral regions.

Discussion

We demonstrated that MRgFUS BBB opening could effectively deliver two small-molecule imaging agents to the CNS. We used two different tracers for GCPII and showed that whether using PET ([^{18}F]DCFPyL) or optical imaging (YC-27), spatially precise and specific

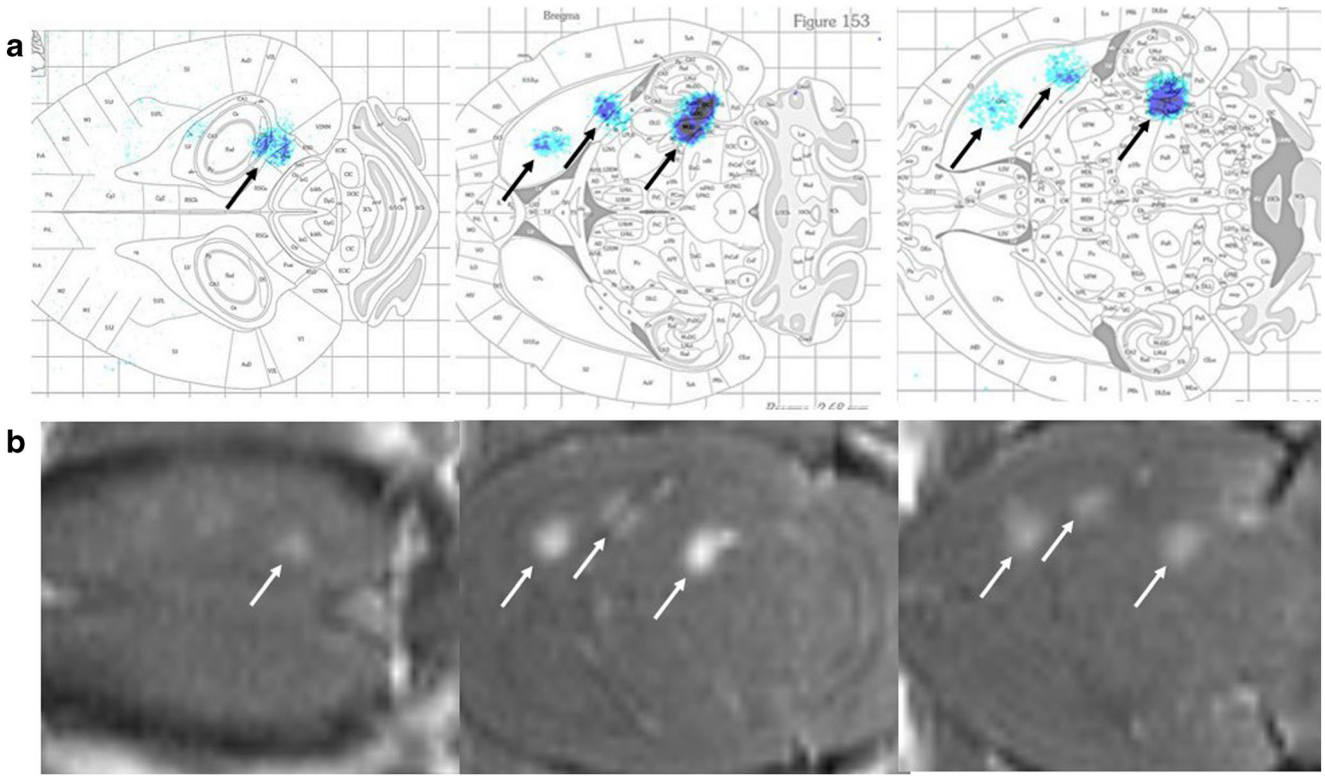

Fig. 3 Autoradiography of [^{18}F]DCFPyL delivered to the brain. BBB opening was completed in three spots of the right hemisphere with increasing estimated *in situ* pressure of 0.45 MPa rostrally, 0.50 MPa in the middle, and 0.55 MPa caudally. **a** Autoradiography demonstrated localization of the foci in the brain with gross overlay onto the Paxinos brain atlas, with agreement with the BBB opening visualized on **b** MRI.

delivery to GCPII in the CNS could be accomplished. This result may enable further investigations of the role of GCPII in a variety of neurological and psychiatric diseases such as gliomas [2]; Alzheimer's disease [3]; and the neurotoxicity associated with schizophrenia, trauma, stroke, and pain [4].

MRgFUS BBB opening has been demonstrated to permit the entry of not only small molecules [17, 21, 34] but also antibodies [22] and even cells [24] to the CNS. Particularly in the case of diagnostics, the issue of washout kinetics from non-target tissue is also an important parameter. Most targeting ligands that are excluded by the BBB are either hydrophilic or >500 Da in molecular weight [36]. Other ligands are substrates for various drug efflux pumps (multidrug resistance (MDR)) [37]. The kinetics of clearance for

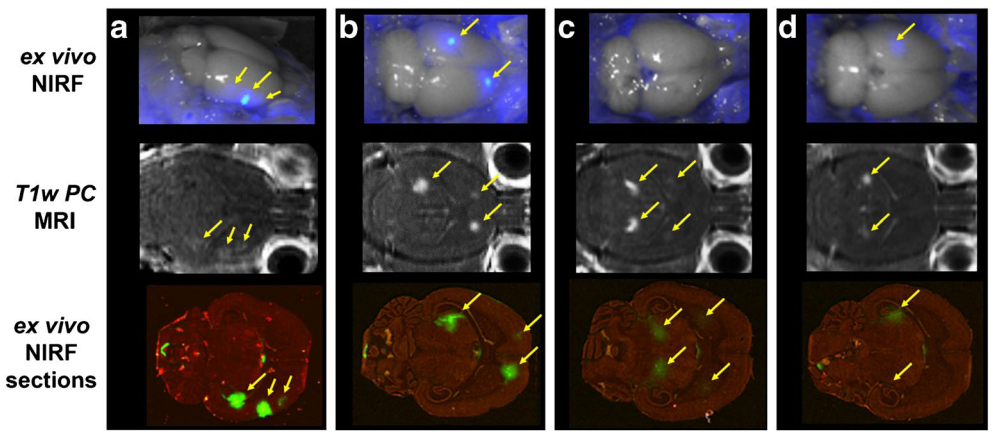

Fig. 4 NIRF imaging demonstrates specific delivery to brain. The optical GCPII/PSMA-targeted agent YC-27 was delivered intravenously without **a**, **b** or with **c**, **d** a blocking dose of the non-fluorescent competitive agent ZJ-43. Both *in situ* (*top*) and post-transverse slice (*bottom*) fluorescent imaging demonstrated adequate penetration of the optical tracer to the CNS (*yellow arrows*), in close correlation with BBB opening as visualized by post-contrast MRI (*middle*, *yellow arrows*). Specific uptake by the brain GCPII target sites is denoted by the marked reduction of signal with ZJ-43 (Color figure online).

small, hydrophilic ligands as well as substrates for drug efflux pumps is expected to be rapid *via* return to the blood pool or circulating CSF. MRgFUS generates a permeable barrier for several hours under the conditions described here and elsewhere [21], which may facilitate both entry and exit of unbound ligands. Therefore, in principle, the techniques described here may be extended to a variety of molecular imaging and theranostic agents that span size ranges from small molecules to gene-carrying nanoparticles. Indeed, for clinical translation, it is likely that that this technique would need to be extended for use with a theranostic and not just diagnostic agent.

Future directions for this technique will establish its versatility. Given recent progress in demonstrating clinical MRgFUS opening of the BBB [20], there is important work to be accomplished for translation of results similar to these to a clinical setting using a variety of clinical MRgFUS transducers [38].

Conclusions

MRgFUS BBB opening is a promising technology for site-specific delivery of molecular imaging and theranostic agents to the CNS, as demonstrated here for the specific case of the delivery of GCPII/PSMA tracers.

Acknowledgments. The authors are grateful for grant and in-kind support for this research from Philips Healthcare, the Walter and Mary Ciceric Foundation, and the National Institutes of Health (grant numbers: CA134675, CA184228). The authors also wish to acknowledge the Johns Hopkins Cyclotron Lab for the provision of surplus cGMP [^{18}F]DCFPyL during these studies.

Compliance with Ethical Standards

Conflict of Interest

The authors (RDA, NPKE, KF, MGP) received limited grant funding and support in kind for this work from Philips Healthcare. Under a licensing agreement between Progenics and the Johns Hopkins University, Dr. Pomper is entitled to royalties on an invention described in this article. This arrangement has been reviewed and approved by the Johns Hopkins University in accordance with its conflict of interest policies.

References

1. Parrish KE, Sarkaria JN, Elmquist WF (2015) Improving drug delivery to primary and metastatic brain tumors: strategies to overcome the blood-brain barrier. Clin Pharmacol Ther 97:336–346
2. Wernicke AG, Edgar MA, Lavi E, et al. (2011) Prostate-specific membrane antigen as a potential novel vascular target for treatment of glioblastoma multiforme. Arch Pathol Lab Med 135:1486–1489
3. Kim M-J, Chae SS, Koh YH, et al. (2010) Glutamate carboxypeptidase II: an amyloid peptide-degrading enzyme with physiological function in the brain. FASEB J 24:4491–4502
4. Bařinka C, Rojas C, Slusher B, Pomper M (2012) Glutamate carboxypeptidase II in diagnosis and treatment of neurologic disorders and prostate cancer. Curr Med Chem 19:856–870
5. Szabo Z, Mena E, Rowe SP, et al. (2015) Initial evaluation of [(18)F]DCFPyL for prostate-specific membrane antigen (PSMA)-targeted PET imaging of prostate cancer. Mol Imaging Biol 17:565–574
6. Eiber M, Weirich G, Holzapfel K, et al. (2016) Simultaneous (68)Ga-PSMA HBED-CC PET/MRI improves the localization of primary prostate cancer. Eur Urol. doi:10.1016/j.eururo.2015.12.053
7. Rai BP, Baum R, Patel A, et al. (2016) The role PET with (68)gallium (Ga)-labelled prostate-specific membrane antigen (PSMA) in the Management of Patient with organ confined and locally advanced prostate cancer prior to radical treatment and after radical prostatectomy. Urology. doi:10.1016/j.urology.2015.12.048
8. Haberkorn U, Eder M, Kopka K, et al. (2016) New strategies in prostate cancer: prostate-specific membrane antigen (PSMA) ligands for diagnosis and therapy. Clin Cancer Res 22:9–15
9. Lütje S, Heskamp S, Cornelissen AS, et al. (2015) PSMA ligands for radionuclide imaging and therapy of prostate cancer: clinical status. Theranostics 5:1388–1401
10. Chen Y, Pullambhatla M, Foss CA, et al. (2011) 2-(3-{1-Carboxy-5-[(6-[18F]fluoro-pyridine-3-carbonyl)-amino]-pentyl}-ureido)-pentanedioic acid, [18F]DCFPyL, a PSMA-based PET imaging agent for prostate cancer. Clin Cancer Res 17:7645–7653
11. Wroblewska B, Santi MR, Neale JH (1998) N-acetylaspartylglutamate activates cyclic AMP-coupled metabotropic glutamate receptors in cerebellar astrocytes. Glia 24:172–179
12. Berger UV, Luthi-Carter R, Passani LA, et al. (1999) Glutamate carboxypeptidase II is expressed by astrocytes in the adult rat nervous system. J Comp Neurol 415:52–64
13. Sácha P, Zámecník J, Barinka C, et al. (2007) Expression of glutamate carboxypeptidase II in human brain. Neuroscience 144:1361–1372
14. Wang H, Byun Y, Barinka C, et al. (2010) Bioisosterism of urea-based GCPII inhibitors: synthesis and structure-activity relationship studies. Bioorg Med Chem Lett 20:392–397
15. Ferraris DV, Majer P, Ni C, et al. (2014) δ-Thiolactones as prodrugs of thiol-based glutamate carboxypeptidase II (GCPII) inhibitors. J Med Chem 57:243–247
16. Nance E, Timbie K, Miller GW, et al. (2014) Non-invasive delivery of stealth, brain-penetrating nanoparticles across the blood-brain barrier using MRI-guided focused ultrasound. J Control Release 189:123–132
17. Huang Y, Hynynen K (2010) MR-guided focused ultrasound for brain ablation and blood-brain barrier disruption. Methods Mol Biol 711:579–593
18. McDannold N, Vykhodtseva N, Raymond S, et al. (2005) MRI-guided targeted blood-brain barrier disruption with focused ultrasound: histological findings in rabbits. Ultrasound Med Biol 31:1527–1537
19. Downs ME, Buch A, Sierra C, et al. (2015) Long-term safety of repeated blood-brain barrier opening via focused ultrasound with microbubbles in non-human primates performing a cognitive task. PLoS One 10:e0125911
20. InSightec, Mainprize T (2015) Blood-brain barrier disruption using transcranial MRI-guided focused ultrasound. In: Clin. Natl. Libr. Med. https://clinicaltrials.gov/ct2/show/NCT02343991.
21. Burgess A, Hynynen K (2013) Noninvasive and targeted drug delivery to the brain using focused ultrasound. ACS Chem Neurosci 4:519–526
22. Kinoshita M, McDannold N, Jolesz FA, Hynynen K (2006) Noninvasive localized delivery of Herceptin to the mouse brain by MRI-guided focused ultrasound-induced blood-brain barrier disruption. Proc Natl Acad Sci U S A 103:11719–11723
23. Hsu P-H, Wei K-C, Huang C-Y, et al. (2013) Noninvasive and targeted gene delivery into the brain using microbubble-facilitated focused ultrasound. PLoS One 8:e57682
24. Burgess A, Ayala-Grosso CA, Ganguly M, et al. (2011) Targeted delivery of neural stem cells to the brain using MRI-guided focused ultrasound to disrupt the blood-brain barrier. PLoS One 6:e27877
25. Mullin L, Gessner R, Kwan J, et al. Effect of anesthesia carrier gas on *in vivo* circulation times of ultrasound microbubble contrast agents in rats. Contrast Media Mol Imaging 6:126–131
26. O'Reilly MA, Muller A, Hynynen K (2011) Ultrasound insertion loss of rat parietal bone appears to be proportional to animal mass at submegahertz frequencies. Ultrasound Med Biol 37:1930–1937
27. Song J, Klibanov AL, Hossack JA, Price RJ (2008) Acoustic attenuation by contrast agent microbubbles in superficial tissue markedly diminishes petechiae bioeffects in deep tissue. Investig Radiol 43:322–329
28. Alkins R, Burgess A, Ganguly M, et al. (2013) Focused ultrasound delivers targeted immune cells to metastatic brain tumors. Cancer Res 73:1892–1899

29. Paefgen V, Doleschel D, Kiessling F (2015) Evolution of contrast agents for ultrasound imaging and ultrasound-mediated drug delivery. Front Pharmacol 6:197
30. Bayer-Healthcare (2016) Magnevist Package Insert. http://labeling.bayerhealthcare.com/html/products/pi/Magnevist_PI.pdf.
31. Jacobson M, Levkovitz R, Ben-Tal A, et al. (2000) Enhanced 3D PET OSEM reconstruction using inter-update Metz filtering. Phys Med Biol 45:2417–2439
32. Chen Y, Dhara S, Banerjee SR, et al. (2009) A low molecular weight PSMA-based fluorescent imaging agent for cancer. Biochem Biophys Res Commun 390:624–629
33. McDannold N, Arvanitis CD, Vykhodtseva N, Livingstone MS (2012) Temporary disruption of the blood-brain barrier by use of ultrasound and microbubbles: safety and efficacy evaluation in rhesus macaques. Cancer Res 72:3652–3663
34. Burgess A, Shah K, Hough O, Hynynen K (2015) Focused ultrasound-mediated drug delivery through the blood–brain barrier. Expert Rev Neurother 15:477–491
35. Yamamoto T, Hirasawa S, Wroblewska B, et al. (2004) Antinociceptive effects of N-acetylaspartylglutamate (NAAG) peptidase inhibitors ZJ-11, ZJ-17 and ZJ-43 in the rat formalin test and in the rat neuropathic pain model. Eur J Neurosci 20:483–494
36. Pardridge WM (1997) Drug delivery to the brain. J Cereb Blood Flow Metab 17:713–731
37. Calias P, Banks WA, Begley D, et al. (2014) Intrathecal delivery of protein therapeutics to the brain: a critical reassessment. Pharmacol Ther 144:114–122
38. Airan RD, Clement GT, Partanen A, et al. (2015) Expanding the treatment envelope for transcranial MR-guided focused ultrasound with a 256-element clinical transducer. ISMRM Conf. Proc.